Alexandria Engineering Journal (2023) 69, 177–191

HOSTED BY

Alexandria University

Alexandria Engineering Journal

www.elsevier.com/locate/aej
www.sciencedirect.com

ORIGINAL ARTICLE

Natural convection heat transfer in a nanofluid filled L-shaped enclosure with time-periodic temperature boundary and magnetic field

Khalid B. Saleem [a], Alia H. Marafie [b,*], Khaled Al-Farhany [c], Wisam K. Hussam [d], Gregory J. Sheard [e]

[a] *Department of Mechanical Engineering, College of Engineering, University of Basrah, Basrah, Iraq*
[b] *Mechanical Engineering Department, College of Engineering and Petroleum, Kuwait University Sabah Al Salem University City, Kuwait*
[c] *Department of Mechanical Engineering, University of Al-Qadisiyah, Al-Qadisiyah, Iraq*
[d] *School of Engineering, Australian University, Safat, Kuwait*
[e] *Department of Mechanical and Aerospace Engineering, Monash University, VIC 3800, Australia*

Received 3 June 2022; revised 28 October 2022; accepted 14 December 2022
Available online 22 December 2022

KEYWORDS

L-Shaped cavity;
Nanofluid;
Oscillating temperature;
Magnetic field

Abstract The natural convective Cu-water nanofluid flow in L-shape cavity with an oscillating temperature profile is studied numerically. The cavity's lower horizontal and left vertical walls are heated sinusoidally with time about a high mean temperature ($\bar{T}_H$). In contrast, the cavity's right vertical wall and its nearby horizontal lower wall are kept cold at a temperature (T_c). The calculations have been performed over temperature oscillation amplitude ($0 \le A \le 2$), dimensionless temperature oscillation frequency ($0 \le f \le 100$), Rayleigh number ($10^3 \le Ra \le 10^8$), Hartmann number ($0 \le Ha \le 100$), the nanoparticles volume fraction ($0 \le \phi \le 0.2$), and enclosure aspect ratios ($0.2 \le AR \le 0.8$). Outcomes reveal that with $AR = 0.2$, heat transfer happens considerably through conduction at $Ra = 10^3$ –10^5, while the time average Nusselt number (Nu) is independent of both Ha and Ra. Convection effects, on the other hand, become significant at high Ra. Additionally, as Ha ascends from 0 to 50, $\bar{N}u$ increases linearly with increasing ϕ, while it remains steady at $Ha = 75$ and 100.

1. Introduction

In recent years, the steady/unsteady-state heat transport within various simple/complex shape cavities has been extensively studied. A new review of studies provides a complete overview

* Corresponding author.
E-mail addresses: khalid.saleem@uobasrah.edu.iq (K.B. Saleem), alia.marafie@ku.edu.kw (A.H. Marafie), khaled.alfarhany@qu.edu.iq (K. Al-Farhany), w.alsaadi@au.edu.kw (W.K. Hussam), Greg.Sheard@monash.edu (G.J. Sheard).
Peer review under responsibility of Faculty of Engineering, Alexandria University.

https://doi.org/10.1016/j.aej.2022.12.030

Nomenclature

A	Temperature oscillation amplitude
AR	Enclosure aspect ratio
$\boldsymbol{B}$	Magnetic field vector
B_o	Magnetic field strength
C_p	Specific heat (J kg^{-1} K^{-1})
f	Dimensionless temperature oscillation frequency
g	Gravitational acceleration (m/s^{-2})
H	Cavity height (m)
Ha	Hartmann number
$\boldsymbol{J}$	Electric current density vector
L	Cavity thickness (m)
Nu	Local Nusselt number
$\bar{Nu}$	Time average Nusselt number
k	Thermal conductivity
p	Pressure (Pa)
P	Dimensionless pressure
Pr	Prandtl number
Ra	Rayleigh number
R_m	Magnetic Reynolds number
T	Temperature (K)
t	Time (s)
t_p	Time period (s)
u,v	Velocity components (m s^{-1})
U,V	Dimensionless velocity components
$\boldsymbol{V}$	Velocity vector (m s^{-1})
x,y	Dimensional coordinates (m)
$X,\ Y$	Dimensionless coordinates

Greek symbols

α	Thermal diffusivity (m^2 s^{-1})
β	Coefficient of thermal expansion (K^{-1})
μ	Dynamic viscosity (Pa s)
μ_0	Magnetic permeability of free space
ν	Kinematic viscosity (m^2 s^{-1})
ω	Angular frequency (s^{-1})
ϕ	Solid volume fraction
Φ	Electric potential
ρ	Density (kg m^{-3})
σ	Electrical conductivity
θ	Dimensionless temperature
τ	Dimensionless time
τ_p	Dimensionless time period

Subscripts

c	Cold magnetic permeability of free space
cr	Critical
h	Hot
f	Fluid
nf	Nanofluid
np	Nanoparticle

of the flow field and heat transfer with/without nanofluid in various geometries of cavities [1–3].

Various solutions were considered to enhance convective heat transfer in many types of equipment [4,5], increasing, for example, the heating system efficiency and cost savings [6]. Various modifications were considered, such as changing the geometry and the boundary conditions [7], utilizing fins [8] and vortex generators [9], and many others. The L-shaped cavity produces a circulation area and vortices [10] that enhance the heat transfer [11]; combined with the use of nanofluid [12], it optimizes the performance of many engineering systems.

In several investigations, nanofluid flows and heat transfer within different shaped cavities have been studied numerically [13–18]. Using a nanofluid-equipped L-shaped enclosure, Mahmoodi [19] numerically studied free convection fluid flow phenomena. The governing equations were discretized using the finite volume method, with the velocity and pressure fields computed using the SIMPLER technique. Various $Ra = 10^3$–10^6, $AR = 0.2$–0.6, as well as $\phi = 0$–0.1, were used in this investigation. Their results showed that when raising the Ra and ϕ, for all cavities' aspects ratios, $\bar{Nu}$ increased.

Sourtiji and Hosseinizadeh [20] employed nanofluids to augment heat transfer in a cavity with L-shaped subjected to magnetohydrodynamics (MHD) natural convection heat transmission effects in the horizontal direction. Their research revealed that AR determines a critical Ra value. Moreover, the existence of the magnetic field affects heat transport and the flow field significantly in cavities, where the $\bar{Nu}$ decreases as the Ha increases. This was due to the Lorentz force, which acts to dampen fluid motion across magnetic field lines.

Utilizing the Lattice Boltzmann Method (LBM), Kalteh and Hasani [21] inspected free convective nanofluid flow in an L-shaped cavity. According to their findings, the nanofluid increases the rate of heat transfer, which is improved with lessening AR. Additionally, increasing the diameter of the nanoparticles has the opposite impact on $\bar{Nu}$.

Mliki et al. [22,23] also utilized the LBM to investigate the heat transfer inside L-shaped chambers with nanofluids. Their research employed two different kinds of nanoparticles (Cu and Al_2O_3). They investigated the effects of several relevant characteristics such as AR, Ha, and Ra on the $\bar{Nu}$. The findings indicate that nanofluid increases the quantity of heat transferred and that decreasing AR boosts this impact.

Mohebbi and Rashidi [24] have implemented a heating obstacle containing nanofluid in an L-shaped enclosure. They elucidated that, for the examined range of Ra, the greater $\bar{Nu}$ is obtained for a high-volume fraction. Furthermore, it increased as AR and the nanoparticles' diameter were reduced. The authors showed that the $\bar{Nu}$ reached its maximum value when placing the heating element within the left wall, in a lower position.

The thermophoresis and the Brownian motion effects on fluid flow and natural convective heat transfer in an L-shaped cavity utilizing nanofluid were investigated by Sheikholeslami et al. [25]. Based on the outcomes, $\bar{Nu}$ ascended by increasing the Rayleigh and the Lewis number, while it

decreased by increasing the AR and the concentration. Using the LBM, Rahimi et al. [26] numerically investigated the free convective flow of a hybrid nanofluid in a hollow L-shaped cavity. The thermophysical characteristics of a SiO_2/TiO_2/water-Ethylene-glycol-nanofluid were found experimentally, resulting in a decrease in the overall entropy production with the enlargement of nanoparticles loading.

The fluid flow, heat transfer by natural convective, and irreversibility in a finned L-shaped enclosure filled with nanofluid were investigated numerically and experimentally by Zhang et al. [27]. The thermal conductivity of TiO_2-SiO_2/W-EG and the dynamic viscosity were found experimentally, whereas the LBM was used for the numerical solution. The cavity's horizontal walls were insulated, while the other walls were maintained at different temperatures. The walls were mounted with four rectangular fins, two of which were hot and the other two were cold. They found that the thermal designs of the implanted fins substantially influenced both the fluid flow and temperature fields.

The AL_2O_3/water nanofluid convection thermo-gravitational within an L-shaped cavity containing a rectangular hot barrier was numerically considered using the LBM by Mohebbi et al. [28]. The impact of various essential factors on the process of cooling and fluid circulation within the cavity were investigated; the nanoparticle volume fractions ($0 \leq \phi \leq 5$ %), the Rayleigh number ($10^3 \leq Ra \leq 10^6$), the aspect ratio ($0.2 \leq AR \leq 0.6$), as well as the height and the position of the heater. According to the findings, the $\bar{Nu}$ increased as the Ra, and ϕ increased, while the rates of heat transfer were discovered to depend strongly on the location of the heating part.

Another interesting numerical investigation of using an open inclined L-shaped cavity containing Ag/water was conducted by Armaghani et al. [29]. They investigated at how heat transport and irreversibility were influenced by the position of the separate hot source. They found that the angle of inclination has a substantial impact on the transport of heat.

A numerical analysis of free convective flow in an L-shaped container using a flexible baffle was performed by Ghalambaz et al. [30]. An Arbitrary Lagrangian-Eulerian moving mesh frame was used numerically to present the governing equations where FEM has been used. The results show that a stiffer baffle slows the heat convective heat by resisting fluid movement. Zhang et al. [31] looked at entropy distributions on the free convective flow with magnetohydrodynamics in an L-shaped enclosure containing Newtonian/non-Newtonian fluids using the finite-difference lattice Boltzmann model (FDLBM). Ahmed et al. [32] investigated MHD Ferro-convection heat transmission in an oblique L-shaped container heated on the corner with a double-lid drive. The flow domain has a heat generation/absorption source, whereas thermal radiation is ignored. The results show that the isothermal distribution increased sharply as the heated corner lengths increased. At constant heat generation parameter ($Q = 2$), when the lengths of the active sections are adjusted between 0.2 and 0.8, $\bar{Nu}$ decreases by 4.7 percent. In addition, as the Hartmann number increases from 0 to 50, the heat transfer is decreased by 30.7 percent for ferrofluid condition with a concentration of 5 percent.

Seyyedi et al. [33] have provided the economic analyses and the entropy generation of convective Al_2O_3-water nanofluid flow within an L-shaped container under the impact of an oriented magnetic field. Their study elucidated that increasing the nanoparticles' loading from 0 to 0.1 decreases the entropy generation by 15.14 percent for $Ha = 25$, while for $Ha = 75$, it decreases by 8.15 percent. Nia et al. [34] utilized the LBM to evaluate the influence of different baffle designs, such as baffle length and location, on the free convection of Cu-water nanofluid fluid flow and transfer of heat within an L-shaped cavity with Ra (10^3 –10^5) and ϕ (0–0.05). According to their finding, the addition of a baffle improves natural convection regardless of its length at lower Ra values, whereas for higher Ra, only the longer baffle, regardless of its location, can improve natural convection.

Recently several studies investigated convective heat transmission and fluid flow in L-shaped porous enclosures with/without nanofluids [35–37]. Using the Buongiorno two-phase model, Chamkha et al. [36] numerically explored the irreversibility and thermal analyses in a permeable L-shaped enclosure filled with nanofluids. A house code was written in C^{++} and added to the Open Foam solver for achieving entropy generation and Buongiorno's model. The results showed that the optimum thermal performance occurred in a 0.5 aspect ratio cavity with Al_2O_3 and CuO nanoparticles. Moria [37] performed a numerical investigation on the influence of heating and porous blocks on the heat transmission and flow of fluid features within an L-shaped enclosure for numerous relevant factors like Ra, Darcy number (Da), enclosure inclination angle, and porous block effective thermal conductivity. According to the heating position, blocks had a considerable influence on the heat transmission rates within the enclosure. Furthermore, the porous block was created to improve the transfer of heat within the cavity.

Almeshaal et al. [38] considered the effects of Ra, Ra, ϕ on Rayleigh-Bénard convective fluid flow with heat transmission and in a three-dimensional L-shaped cavity involving nanofluid (MWCNT-water). For Ra values, less than 10^5 and 3 percent of nanoparticle fractions, the AR of 0.4 gives optimum heat transfer. The AR and the percentage of nanoparticles were increased to improve the 3-D appearance.

Recently, LBM was used by Mohammadifar et al. [39] to investigate laminar free convective Cu/water nanofluid flow in an L-shape enclosure with an open end. The impact of Ra, AR, and ϕ on heat transfer and fluid flow were examined using various boundary conditions at the east side of the open-end enclosure. The most significant heat transfer improvement of 186.92 percent was reached when the boundary conditions were changed from a fixed adiabatic wall to an open boundary condition. The oblique magnetic field effects on heat transport and irreversibility within an L-shaped cavity occupied with alumina/water were studied by Zhang et al. [40]. The cavity's L-shape was modeled as a circle's quadrant. The results indicated that for high values of Ra, the perpendicular magnetic field attained the maximum rates of irreversibility and transfer of heat.

Armaghani et al. [41] considered the impact of the heat sink/source size and position on an L-shaped cavity having MHD mixed convection and filled with Al_2O_3-Cu/Water hybrid nanofluid. The findings show that using the highest sink power resulted in the optimum heat transfer.

As this review reveals, most studies supposed uniform temperatures at the walls of the L-shaped cavity. However, several applications in engineering are subject to a variable tempera-

ture, such as energy storage, thermal insulation in buildings, and solar thermal systems. System's walls with recirculating fluid under different conditions have grasped many researchers' attention. The importance is rising in many industrial sectors, such as optimizing the design of heat exchangers and energy recovery systems. To the best of our knowledge, the influence of time-periodic boundary temperature and magnetic field in an L-shaped cavity filled with nanofluid has not been studied in the literature. Therefore, the main objective of this study is to investigate the effect of different parameters (Rayleigh number, aspect ratio of the cavity, Hartmann number) on fluid flow and temperature fields and the corresponding heat transfer features within the L-shaped cavity subjected to time-varying thermal boundaries.

2. Problem statement and mathematical formulation

The configuration of the current work, elucidated in Fig. 1, involves a 2-dimensional L-shaped cavity of equal width and height H with a thickness L and aspect ratio $AR = L/H$. The cavity is filled with Cu-water nanofluid with Prandtl number Pr of 6.2. Cu-water nanofluid has been selected as the working fluid inside the cavity as they are widely used as coolants in industrial applications. For example, adding copper nanoparticles of $\phi = 0.003$ to ethylene glycol has increased thermal conductivity by 40 % [42].

The left vertical and the perpendicular lower walls are exposed to an unsteady temperature condition that varies sinusoidally with time (t) and has an average high temperature of $\bar{T}_h$, angular frequency ω, and temperature oscillation amplitude A, and expressed as:

$$T(t) = \bar{T}_h + A\sin\omega t \tag{1}$$

The outer walls of the L-shape are hot, and the inner walls are cold, with the ends being adiabatic. A uniform magnetic field of a strength B_o is exerted in the positive direction of x-axis and permeates through the nanofluid. Those two conditions provide a combination of electromagnetic force and buoyancy forces that control the produced convective fluid flow. An electrically conducting fluid does not produce a magnetic field. The impact of the thermal Joule heating and viscous dissipation of the fluid are likewise neglected. Table 1 details the thermophysical properties of the carrier fluid (water) and the Cu-nanoparticle. For the fluid buoyancy, the Boussinesq approximation is used, where density differences within the fluid are ignored, with the exception of the gravitational force expression in the y-momentum equation.

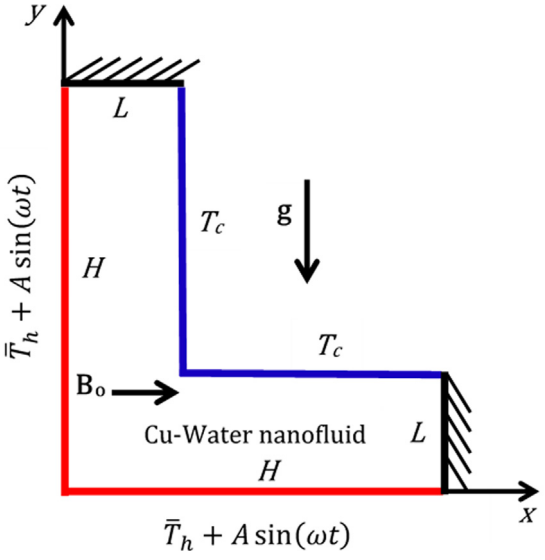

Fig. 1 Schematic for the studied configuration.

2.1. Governing equations

According to the previously described assumptions, for an unsteady-two-dimensional Cartesian coordinate system, the conservation equations comprise a mass conservation equation, horizontal and vertical momentum equations and an energy equation that are respectively written as

$$\frac{\partial u}{\partial x} + \frac{\partial v}{\partial y} = 0, \tag{2}$$

$$\frac{\partial u}{\partial t} + u\frac{\partial u}{\partial x} + v\frac{\partial u}{\partial y} = -\frac{1}{\rho_{nf}}\frac{\partial p}{\partial x} + \nu_{nf}\left(\frac{\partial^2 u}{\partial x^2} + \frac{\partial^2 u}{\partial y^2}\right), \tag{3}$$

$$\frac{\partial v}{\partial t} + u\frac{\partial v}{\partial x} + v\frac{\partial v}{\partial y} = -\frac{1}{\rho_{nf}}\frac{\partial p}{\partial y} + \nu_{nf}\left(\frac{\partial^2 v}{\partial x^2} + \frac{\partial^2 v}{\partial y^2}\right) + \frac{1}{\rho_{nf}}(\rho\beta)_{nf} g(T - T_c) - \frac{\sigma_{nf} B^2 v}{\rho_{nf}}, \tag{4}$$

$$\frac{\partial T}{\partial t} + u\frac{\partial T}{\partial x} + v\frac{\partial T}{\partial y} = \alpha_{nf}\left(\frac{\partial^2 T}{\partial x^2} + \frac{\partial^2 T}{\partial y^2}\right). \tag{5}$$

The thermophysical properties of the nanofluids are included in the governing Eqs. (2–5); density (ρ_{nf}), kinematic viscosity (ν_{nf}), electrical conductivity (σ_{nf}), coefficient of thermal expansion (β_{nf}) and thermal diffusivity (α_{nf}), are represented in section 2.3. The magnetic field (B) is discussed in section 2.2.

2.2. Electromagnetic forces

The Lorentz force $\boldsymbol{J} \times \boldsymbol{B}$, which is defined as the vector cross product of the density of the electric current ($\boldsymbol{J}$) and magnetic field ($\boldsymbol{B}$), describes the influence of electromagnetic fields in the momentum equation. This work proceeds under the assumption that flows herein satisfy the low magnetic Reynolds number assumption ($R_m = ul\sigma\mu_0 \ll \|l$), where $\mu_0 = 1.2566\times 10^{-6}\mathrm{kg\,m\,s^{-2}\,A^{-2}}$ is the magnetic permeability of free space, u and l are characteristic velocity and length scales, and σ is

Table 1 Thermophysical properties of water and Cu-nanoparticles [43].

Property	Water	Cu
ρ (kg/m^3)	997.1	8933
C_p (J/kg K)	4179	385
k (W/m K)	0.613	400
$\alpha \times 10^{-7}$ (m^2/s)	1.47	1163.1
$\beta \times 10^{-6}$ (1/K)	210	51

the electrical conductivity [44]. Under this assumption, the electric field may be represented by the gradient of an electric potential field ($\nabla\Phi$). Ohm's law may thus be written as

$$\boldsymbol{J} = \sigma(-\nabla\Phi + \boldsymbol{V} \times \boldsymbol{B}), \tag{6}$$

$$\nabla \cdot \boldsymbol{J} = 0. \tag{7}$$

The electric potential equastion is thus given by

$$\nabla^2\Phi = \boldsymbol{B}_o\left(\frac{\partial \boldsymbol{U}}{\partial \boldsymbol{Y}} - \frac{\partial \boldsymbol{V}}{\partial \boldsymbol{X}}\right). \tag{8}$$

where Φ is the electric potential, $\boldsymbol{V}$ is the velocity vector, and B_o is the strength of the magnetic field which leads to a Poisson equation for the electric potential field. For a 2D velocity field $\boldsymbol{V}(x,y)$ and $\boldsymbol{B}$ acting in the x-direction, $\boldsymbol{V} \times \boldsymbol{B}$ is nonzero only in the z-direction, and its divergence must therefore be zero. This reduces the Poisson equation to

$$\nabla^2\Phi = 0. \tag{9}$$

According to Pirmohammadi et al. [45], for the flow in a cavity with electrically insulating boundaries the electric potential satisfies $\partial\Phi/\partial n = 0$, rendering the solution of Eq. (9) as $\Phi =$ constant, the gradient of which is zero in the Lorentz force, $\boldsymbol{V} \times \boldsymbol{B}$. Thus, only the $\sigma(\boldsymbol{V} \times \boldsymbol{B})$ part of Ohm's law contributes to the Lorentz force, ultimately appearing as $-\sigma_{nf}B^2\boldsymbol{v}/\rho_{nf}$ in the vertical momentum Eq. (4).

The water and nanoparticle electric conductivities are assumed as 0.05 and 5.96×10^7 kg^{-1} m^{-3} s^3 A^2, so that over the computed range of volume fractions, the product of characteristic velocity and length scales required to satisfy the $R_m \ll 1$ assumption range from $(ul)_{\Phi=0} \| 1.59 \times 10^7 \sim \mathrm{m^2 s^{-1}}$ to $(ul)_{\Phi=0.2} \| 6.68 \times 10^{-2} \sim \mathrm{m^2 s^{-1}}$. Thus, it is clear that at smaller volume fractions, the low-R_m assumption is satisfied for any practical industrial speed and length scales, while at the upper end the assumption holds at small scales and low speeds.

2.3. Nanofluids thermophysical properties relations

The nanofluids' thermophysical properties, including the heat capacitance $(\rho C_p)_{nf}$, are to be evaluated by the following relations [46–48]:

$$\rho_{nf} = (1-\phi)\rho_f + \phi\rho_{np}, \tag{10}$$

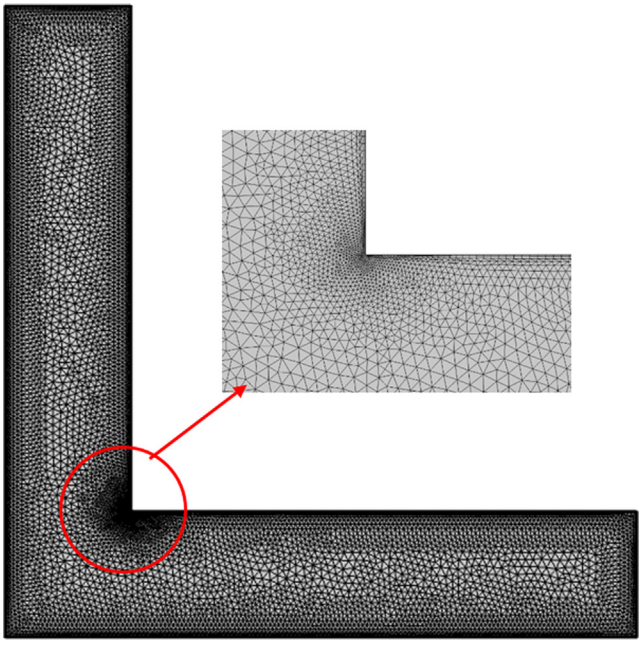

Fig. 2 Schematic for the grid type employed on the study.

Table 3 Code verification for L-shaped cavity utilizing nanofluid with $AR = 0.4$ and $f = 0.06$ with Mahmoodi [19] and Saidi and Karimi [12] findings.

Ra	$\overline{Nu}$-Mahmoodi [19]	$\overline{Nu}$-Saidi and Karimi [12]	$\overline{Nu}$-Present model
10^3	2.137	2.208	2.119
10^4	2.284	2.241	2.196
10^6	7.764	8.007	7.765

Table 4 Code verification for square cavity with Hussam et al. [51] case at $Ra = 10^6$, $A = 2$, $Ha = 25$.

f	$\bar{N}u$- Hussam et al. [51]	$\bar{N}u$- Present study	Relative error (%)
0	11.34	11.37	0.32
0.05	12.29	12.42	1.05
0.10	13.21	13.45	1.84
0.15	14.12	14.49	2.66
0.20	15.05	15.53	3.19

Table 2 Grid sensitivity analysis with $AR = 0.2$, $Ra = 10^6$, $Ha = 100$, $A = 2$, and $f = 1$.

Mesh	Grid number	$\bar{N}u$	Error%	
1	758	18.687	–	
2	1168	18.550	7.41 x10^{-1}	
3	1678	18.467	4.48 x10^{-1}	
4	5170	18.359	5.87 x10^{-1}	
5	14,476	18.344	8.68 x10^{-2}	*selected mesh*
6	36,168	18.343	3.61 x10^{-3}	

$$\sigma_{nf} = (1-\phi)\sigma_f + \phi\sigma_{np}, \tag{11}$$

$$(\rho C_p)_{nf} = (1-\phi)(\rho C_p)_f + \phi(\rho C_p)_{np}, \tag{12}$$

$$(\rho\beta)_{nf} = (1-\phi)(\rho\beta)_f + \phi(\rho\beta)_{np}, \tag{13}$$

$$\alpha_{nf} = \frac{k_{nf}}{(\rho C_p)_{nf}}, \tag{14}$$

with the subscripts (*f*) and (*nf*) denoting the base-fluid and the nanofluid, respectively.

The kinematic viscosity of the nanofluids is expressed as

$$\nu_{nf} = \frac{\mu_{nf}}{\rho_{nf}}, \tag{15}$$

with the effective dynamic viscosity (μ_{nf}) of the nanofluid expressed by the result represented by Brinkman [49] for a fluid that contains suspension of small rigid spherical particles, as

$$\mu_{nf} = \frac{\mu_f}{(1-\phi)^{2.5}}, \tag{16}$$

Also, the nanofluid effective thermal conductivity (k_{nf}) is to be evaluated using the result by Yu and Choi [50], which counts for the liquid nanolayer on the surface of a nanoparticle and is expressed as

$$\frac{k_{nf}}{k_f} = \frac{k_{np} + 2k_f - 2(k_f - k_{np})(1+\eta)^3\phi}{k_{np} + 2k_f + (k_f - k_{np})(1+\eta)^3\phi}, \tag{17}$$

where η is a dimensionless number representing the ratio of the nanolayer thickness to particle's radius, taken as 0.1 in this work [43].

2.4. Normalized governing Equations, Boundary, and initial conditions

Defining the dimensionless parameters,

$$\tau = \frac{\alpha_f t}{H^2}, \quad X = \frac{x}{H}, \quad Y = \frac{y}{H}, \quad U = \frac{uH}{\alpha_f}, \quad V = \frac{vH}{\alpha_f},$$
$$\theta = \frac{T - T_c}{T_h - T_c}, \quad P = \frac{pH^2}{\rho_{nf}\alpha_f^2}, \quad Ha = B_o H\sqrt{\frac{\sigma_{nf}}{\rho_{nf}\nu_f}},$$

$$Ra = \frac{g\beta_f(T_h - T_c)H^3}{\nu_f\alpha_f}, \; Pr = \frac{\nu_f}{\alpha_f}. \tag{18}$$

The normalized forms of the Governing equations, Eqs. (2) – (5), can be written as:

$$\frac{\partial U}{\partial X} + \frac{\partial V}{\partial Y} = 0, \tag{19}$$

$$\frac{\partial U}{\partial \tau} + U\frac{\partial U}{\partial X} + V\frac{\partial U}{\partial Y} = -\frac{\partial P}{\partial X} + \frac{\nu_{nf}}{\alpha_f}\left(\frac{\partial^2 U}{\partial X^2} + \frac{\partial^2 U}{\partial Y^2}\right), \tag{20}$$

$$\frac{\partial V}{\partial \tau} + U\frac{\partial V}{\partial X} + V\frac{\partial V}{\partial Y} = -\frac{\partial P}{\partial Y} + \frac{\nu_{nf}}{\alpha_f}\left(\frac{\partial^2 V}{\partial X^2} + \frac{\partial^2 V}{\partial Y^2}\right) + \frac{(\rho\beta)_{nf}}{\rho_{nf}\beta_f} RaPr\theta - Ha^2 PrV, \tag{21}$$

$$\frac{\partial \theta}{\partial \tau} + U\frac{\partial \theta}{\partial X} + V\frac{\partial \theta}{\partial Y} = \frac{\alpha_{nf}}{\alpha_f}\left(\frac{\partial^2 \theta}{\partial X^2} + \frac{\partial^2 \theta}{\partial Y^2}\right). \tag{22}$$

The normalized initial and boundary conditions utilized in this study are expressed below:

Initial condition:

at $\tau = 0$: $U = V = 0$ (no flow), $\theta = 0$ (uniform T_c though out).

Boundary conditions:

at $X = 0$ and $Y = 0$: $U = V = 0$ (no-slip condition),

$\theta = 1 + Asin\left(\frac{2\pi\tau}{\tau_p}\right)$(imposed sinusoidal temperature).

at $X = \frac{L}{H}$ and $Y = \frac{L}{H}$: $U = V = 0$ (no-slip condition), $\theta = 0$ (surface at T_c)

at $X = 1$ and $Y = 1$: $\quad U = V = 0, \frac{d\theta}{dY} = 0$ (adiabatic surface).

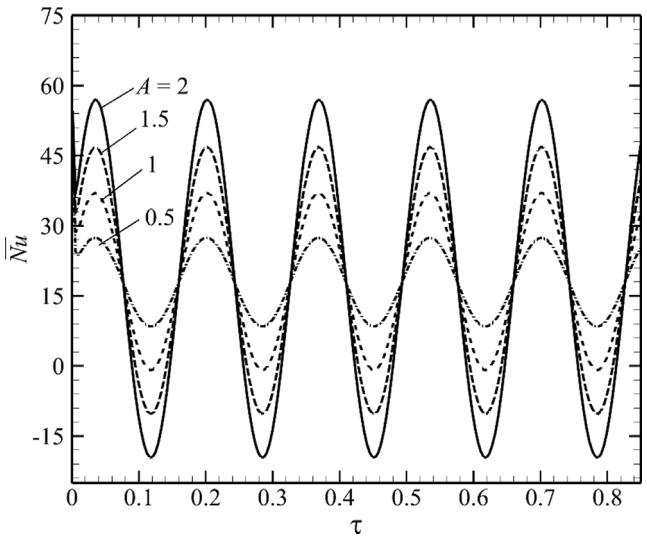

Fig. 3 Transient response of $\bar{Nu}$ for different selected A values for $f = 6$, $AR = 0.2$, $Ra = 10^6$, $Ha = 100$, and $\phi = 0.2$.

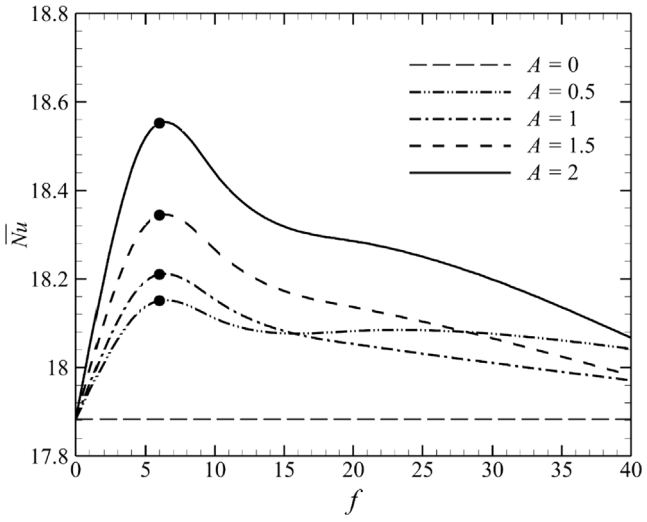

Fig. 4 $\bar{Nu}$ variation for $\phi = AR = 0.2$, $Ra = 10^6$, and $Ha = 100$ for selected A and over a range of f. The horizontal dashed line depicts $\bar{Nu}$ in the absence of oscillation. (●) represents the maximum $\bar{Nu}$ locus as a function of f.

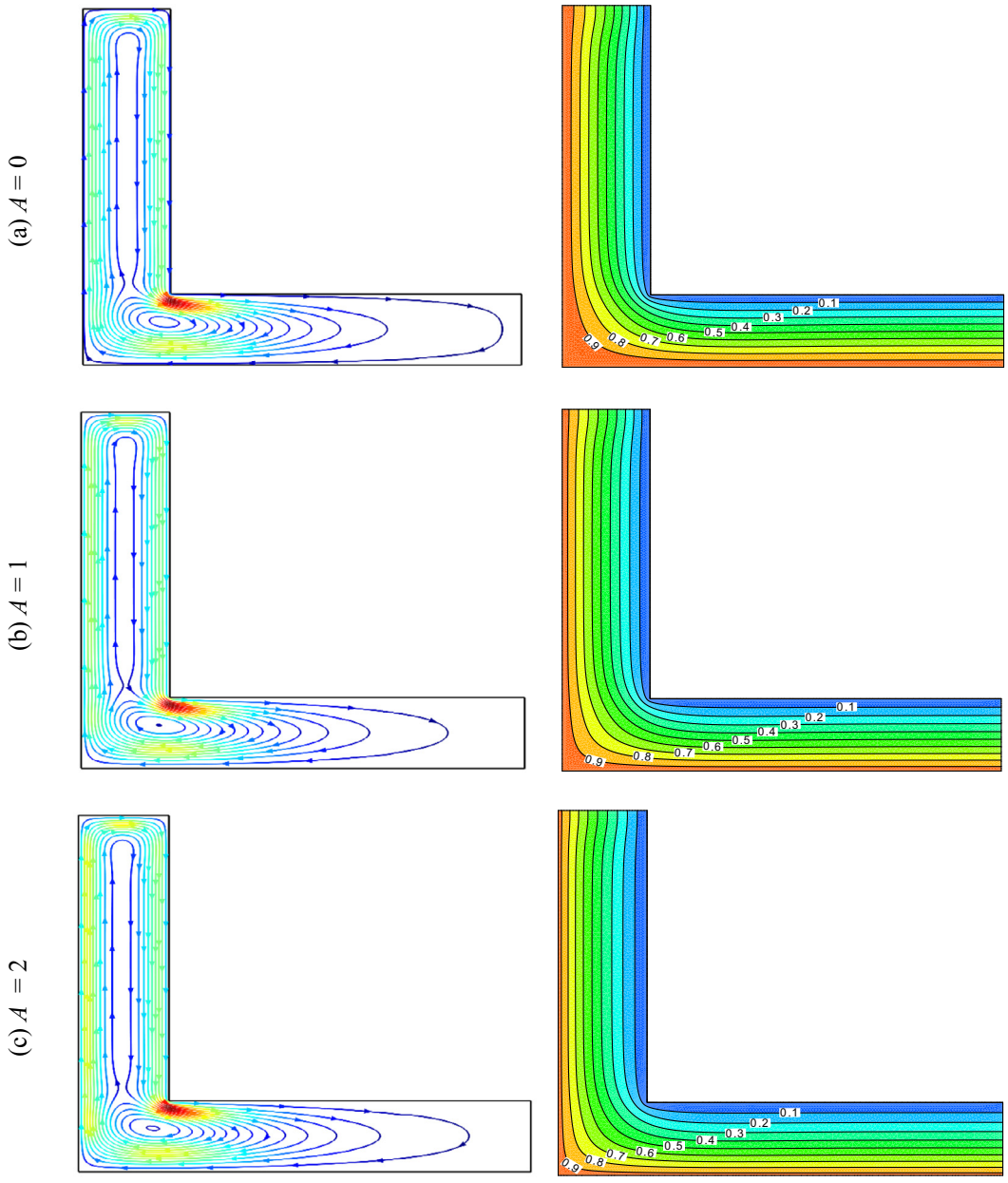

Fig. 5 Left: Streamlines colored for flow speed. Right: Isotherms. Instantaneous contours plot at $f = 6$ after one period of oscillation for $AR = 0.2$, $\phi = 0.2$, $Ra = 10^6$, $Ha = 100$, and selected A. The minimum and maximum levels of velocity magnitudes are (a) 0 to 35, (b) 0.43 to 31.4, and (c) 0.35 to 28.33.

A temperature oscillation amplitude has normalized by $(T_h - T_c)$ whose dimensionless period and frequency are determined by $\tau_p = \frac{\alpha_f t_p}{H^2}$ and $f = \omega H^2/\alpha_f$, respectively, with time period t_p.

The local Nusselt number over the two hot walls is expressed as

$$Nu(Y) = -\left(\frac{k_{nf}}{k_f}\right)\left(\frac{\partial\theta}{\partial X}\right)_{X=0}, \quad \text{and} \quad Nu(X) = -\left(\frac{k_{nf}}{k_f}\right)\left(\frac{\partial\theta}{\partial Y}\right)_{Y=0}. \tag{24}$$

The average value along the two hot walls becomes

$$\overline{Nu} = \frac{1}{2}\left(\int_0^H Nu(Y)dY|_{X=0} + \int_0^H Nu(X)dX|_{Y=0}\right). \tag{25}$$

3. Grid independent and validation

Numerical simulations were performed using the COMSOL Multiphysics package, employing a finite-element method for spatial discretization and a backward differentiation method for time integration. A thorough grid resolution study was conducted to ensure adequate spatial and temporal resolution of the numerical simulations. The grid-type employed in the present study is a triangular grid that illustrated in Fig. 2, and the grid sensitivity is examined by evaluating $\overline{Nu}$ at the heated walls with six grid numbers and with $AR = 0.2$, $Ra = 10^6$, $Ha = 100$, $A = 2$, and $f = 1$, as illustrated in Table 2. The relative error decreases considerably with increas-

ing mesh resolution, which indicates that the reasonable accuracy in results is fulfilled with meshes 5 and 6, and mesh number 5 is selected for use hereafter due to reduced computational expense.

The present formulation is validated against numerous cases. The first case is performed with reference to the results by Mahmoodi [19] and Saidi and Karimi [12] for an L-shaped cavity utilizing a nanofluid without a magnetic field and fixed hot temperature on the heated walls at $AR = 0.4$ and $f = 0.06$ as revealed in Table 3. The current results are in good agreement with the published results.

The second case of verification has been achieved by comparing with Hussam et al. [51] for a square cavity with a periodically varying temperature profile under a magnetic field at $Ra = 10^6$, $Ha = 25$, $A = 2$, as given in Table 4. There is a good agreement between the two models with a maximum relative error of 3.19 percent.

4. Results and discussion

The numerical simulation results of the buoyancy-driven flow in L-shaped cavities filled with Cu-water nanofluid are discussed in this section. The effects of parameters including the temperature oscillation amplitude ($0 \le A \le 2$), the oscillation frequency ($0 \le f \le 100$), the Rayleigh number ($10^3 \le Ra \le 10^8$), the Hartmann number ($0 \le Ha \le 100$), the nanoparticle volume fractions ($0 \le \phi \le 0.2$), and the aspect ratios of the enclosure ($0.2 \le AR \le 0.8$) are investigated. Between 2 and 20 oscillating periods were computed to ensure that the solutions reached a statistical steady state not contaminated by the initial conditions. A time step $\Delta\tau = 0.001$ and integration over 200-time units are used throughout the computations.

Fig. 3 represents the transient response of the average Nusselt number ($\bar{Nu}$) with time during 6 periods of oscillation for selected values of forcing amplitude and with $AR = 0.2$, $Ra = 10^6$, $Ha = 100$, and $\phi = 0.2$. This figure demonstrates that $\bar{Nu}$ changes periodically, a similar pattern as the imposed temperature condition on the heated walls, with the maximum peak value at the largest amplitude of oscillation; this condition enhances the heat transfer significantly.

Fig. 4 depicts the $\bar{Nu}$ variation for $\phi = AR = 0.2$, $Ra = 10^6$, and $Ha = 100$ for selected amplitudes of oscillation and over a range of forcing frequencies. The case with $A = 0$ represents a constant surface temperature condition ($\bar{T}_h$) on the two heated walls; this case corresponds to the lowest value of the $\bar{Nu}$, which is also constant. The effect of the periodic temperature boundary conditions propagates through the cavity, causing an increase in the time-average $\bar{Nu}$, with the highest value corresponding to the larger amplitude for the same frequency. Interestingly, as the amplitude grows, the frequency for maximum $\bar{Nu}$ remains nearly constant ($f \approx 6$) for all amplitudes considered in this study ($A = 0.5, 1, 1.5, 2$). The peak frequency response was different from that of a square cavity, where peak frequency remains constant for $A > 0.5$ while increasing for $A \le 0.5$ [51].

To gain further insight into the results represented in Fig. 4, the streamlines and isothermal contours of natural convection within the enclosure for different amplitudes are plotted in Fig. 5 (using the same parameters as in Fig. 4). The streamline contours show a slow flow near the boundaries, while in the arms of the cavity, the temperature varies almost linearly from the hot boundary to the adjacent cold boundary (a feature consistent with a conduction-dominated flow), and at low amplitudes, the outer corner of the L-bend features a relatively broad warm region, which becomes smaller as amplitude increases. Interestingly, in the vertical arm of the cavity, the streamlines demonstrate that the flow adopts a 1D profile that is invariant in y away from the bend and the end-wall, while in the horizontal arm, the flow circulates with a significant x -dependence.

Also, the pattern of the streamlines changes slightly with the increase in the temperature amplitude. As the maximum amplitude of the oscillation increases, the temperature difference between the cold and hot walls increases. Therefore, the fluid touching the cold surface cools and migrates toward the hot region of the cavity, near the hot walls, due to the buoyancy effect, resulting in substantially improved heat transfer.

Fig. 6 portrays the alteration of the $\bar{Nu}$, at the peak oscillation frequency, with Ra and selected values of Hartmann numbers for $AR = \phi = 0.2$, and $A = 2$. The value of $\bar{Nu}$ progresses with the increase of Ra, for a given value of Ha, a variety of zones can be distinguished from this; the first zone covers the small to moderate range of Rayleigh numbers

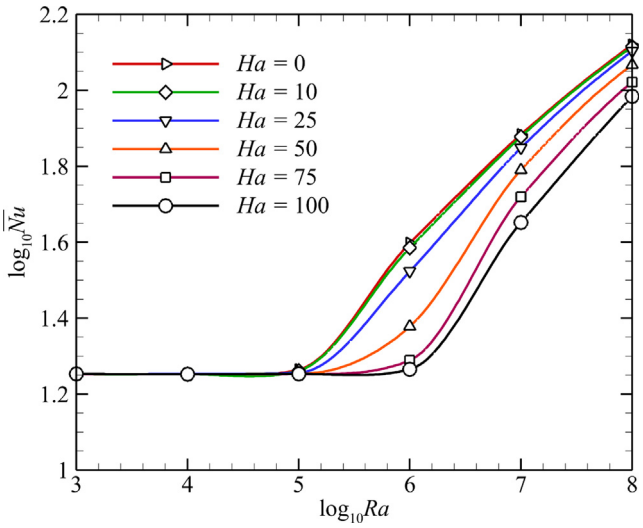

Fig. 6 $\text{Log}_{10}\bar{Nu}$ against $\log_{10}Ra$ plot at $f = 6$ for $AR = \phi = 0.2$ and $A = 2$ for selected Ha. Data are fitted with cubic splines for guidance.

Table 5 Critical Ra values for the departure from the conduction regime with reference to the selected Ha at the peak frequency ($f = 6$) for $AR = \phi = 0.2$ using Eq. (26).

Ha	Ra_{cr}
10	1.04×10^5
25	2.63×10^5
50	5.03×10^5
75	7.26×10^5
100	9.40×10^5

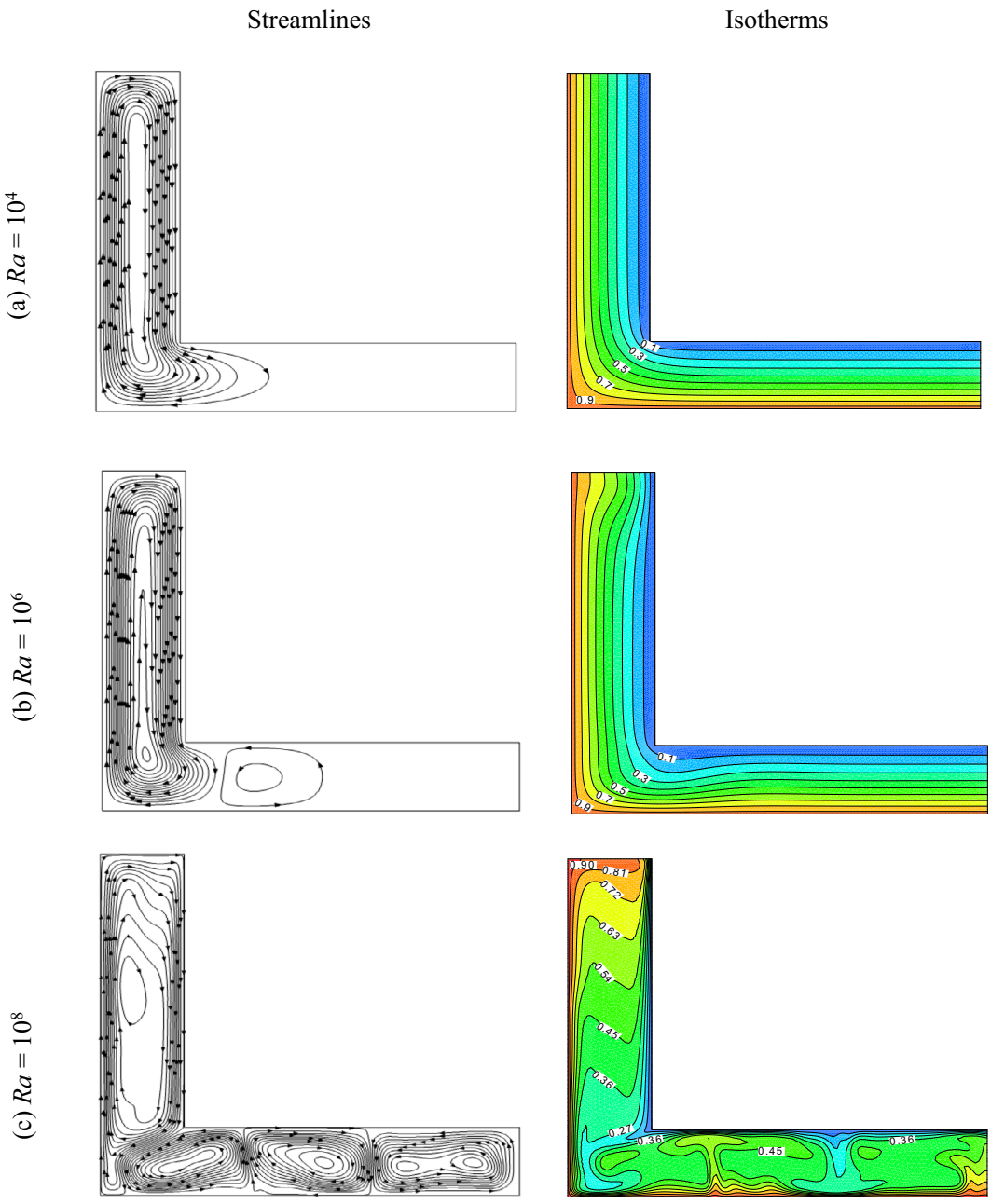

Fig. 7 Instantaneous streamlines and isothermal contours at $f = 6$ with various Ra after one oscillation period and $AR = \phi = 0.2$, $A = 2$, $Ha = 25$ (a) $Ra = 10^4$, (b) $Ra = 10^6$, and (c) $Ra = 10^8$.

($Ra = 10^3$ –10^5), and the second zone covers the high range of $Ra > 10^5$. Through the first zone, $\bar{Nu}$ is nearly constant with negligible effects due to the changes in Ra and Ha; the fluid flow is dominated by diffusion and the heat transfer is dominated by conduction. Also, the hot wall boundaries do not have a clearly visible boundary layer. In the second zone, the $\bar{Nu}$ generally rises significantly as Ra increases and become sensitive to the changes in Ha; the transmission of heat and flow of fluid are dominated through convection. Observing the changes in the $\bar{Nu}$ through the whole region, there is a critical Rayleigh number (Ra_{cr}) for every Ha value beyond which the $\bar{Nu}$ rapidly increases. The Ra_{cr} and Ha data in Fig. 6 were correlated using the power-law correlation with a coefficient $r^2 = 0.9986$ over the range of $10 \leq Ha \leq 100$ and expressed below as:

$$Ra_{cr} = C + DHa^n \tag{26}$$

where $C = -28335.6$, $D = 17987.48$ and $n = 0.8654$. This is based on the buoyancy and Lorentz forces by Ra and Ha in Eq. (21), whose ratio is approximately Ra/Ha^2. Natural convection and Lorentz force are balanced to determine the threshold between them. Table 5 lists the values of different Ha and the corresponding critical Ra, related to the minimum $\bar{Nu}$ at which the departure from conduction to convection starts, obtained by using Eq. (26).

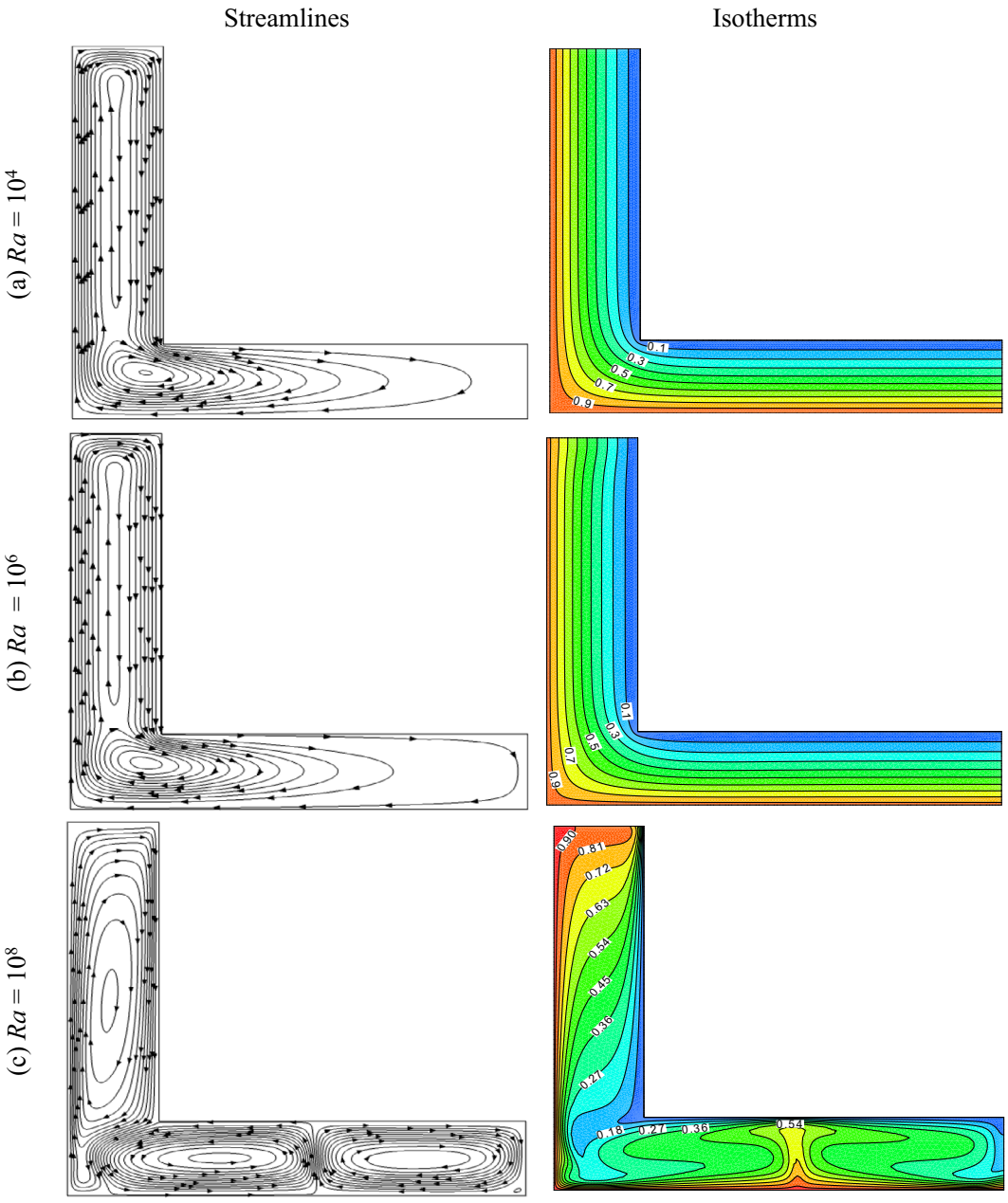

Fig. 8 Instantaneous streamlines and isothermal contours at $f = 6$ with various Ra for one oscillation period and $AR = \phi = 0.2$, $A = 2$, $Ha = 100$ (a) $Ra = 10^4$, (b) $Ra = 10^6$, and (c) $Ra = 10^8$.

The streamlines and isotherms are sketched for distinct Ra and Ha in Fig. 7 ($Ha = 25$) and Fig. 8 ($Ha = 100$). These fields are displayed after one oscillation period for $AR = \phi = 0.2$, and $A = 2$. First, observing the streamlines in Fig. 7, which represents the low Hartmann number case ($Ha = 25$); at low $Ra = 10^4$, two flow regions are formed, the stagnate region in the horizontal segment of the enclosure, whereas the fluid in the vertical segment of the produces a single clockwise rotating vortex. Ascending the temperature variance between the enclosure cold and hot walls causes an increase in the Ra. At $Ra = 10^6$ a counterclockwise rotating vortex is evolved inside the enclosure's horizontal segment; this vortex has features consistent with a Rayleigh-Bénard convection cell, which emerges due to the unstable vertical buoyancy gradient in this region. With a further increase in the Rayleigh number to $Ra = 10^8$, the number of the alternately rotating vortices increases to three resulting in a substantial improvement in the transfer of heat and hence the Nusselt number. Fig. 8 presents the high Hartmann number case ($Ha = 100$); at low to moderate Ra values of 10^4 and 10^6, two secondary clockwise rotating vortices are embedded within the primary vortex that occupies the whole enclosure. At $Ra = 10^8$, clockwise and counterclockwise rotating vortices are formulated on the horizontal segment of the enclosure. It is apparent when comparing the $Ra = 10^8$ data at $Ha = 100$ (Fig. 8c) against the $Ha = 25$ case (Fig. 7c) that the relatively stronger Lorentz force in the $Ha = 100$ case is inhibiting the vertical convective motion of the Rayleigh-Bénard convection cells, resulting in a

smaller number of broader cells when compared to the $Ha = 25$ case.

Secondly, observing the isotherm lines in both cases of low and high *Ha,* as shown in Figs. 7 and 8, at $Ra = 10^4$ and 10^6, the developed isotherm lines are primarily parallel to the non-adiabatic walls of the enclosure and characterize a diffusion-dominated regime resulting in heat transfer mainly by conduction. With a further increase in the buoyancy force within the cavity at $Ra = 10^8$, numerous thermal boundary layers are produced in the vicinity of the non-adiabatic walls, characterized by a convective-dominated regime resulting in heat transfer mainly by convection. For $Ha = 25$, it can be noted that after $Ra = 10^5$, the flow transitions from diffusion-dominated to convection-dominated regimes. For $Ha = 100$, however, the flow continues in a diffusion-dominated regime for $Ra < 10^6$, followed by transitions to a convective-dominated regime beyond $Ra = 10^6$ owing to the ascend in buoyancy force. Furthermore, for both values of *Ha* and at $Ra = 10^8$, the isotherm lines slope from the non-adiabatic walls in the vertical portion of the enclosure; however, it has an irregular shape in the horizontal portion due to the stronger convective effects replacing the smoother diffusion-dominated features.

The $\bar{Nu}$ variation with the nanoparticle volume fraction (ϕ) for selected Hartmann number, at the peak frequency, with $AR = 0.2$, $Ra = 10^6$ and $A = 2$, is depicted in Fig. 9. In general, $\bar{Nu}$ ascends with Φ enlargement; due to the fact that using Cu-water nanofluid is thermally more conductive than pure fluid casing an increase in the transfer of heat. Additionally, it is realized that the gradient of the trends slope changes substantially as the *Ha* increases from 10 to 100. The growth is more identifiable at low Hartmann numbers; the $\bar{Nu}$ augments linearly with enlarging nanoparticle loading as *Ha* increases from 0 to 50, while it remains nearly constant at $Ha = 75$ and 100. This result may be attributed to the Lorentz force damping the buoyant flows of nanofluid with high nanoparticle concentrations, which reduces the heat transfer by convection.

The $\bar{Nu}$ variation with the aspect ratio (AR) for selected Hartmann number, at the peak frequency, with $\phi = 0.2$, $Ra = 10^6$, and $A = 2$, is depicted in Fig. 10. It is observed that as AR varies from $AR = 0.2$ to 0.8, for a given *Ha*, there is a remarkable drop in the $\bar{Nu}$. However, for a given AR value, smaller Hartmann number $Ha = (0, 10, 25)$ produce the largest $\bar{Nu}$ values. Additionally, the variance in $\bar{Nu}$ between the cases of $Ha = 0$ (no magnetic field) versus $Ha = 100$ (largest effect of magnetic field) lessens with the rise in AR. The transfer of heat enhances as AR decreases, and this increase becomes more pronounced in the range of $Ha \leq 25$ by almost 64 %. However, for low values of $Ha \leq 10$, the effect of the Ha on $\bar{Nu}$ is negligible regardless of the aspect ratio. To furtherly explain these conditions, the streamlines and isotherms contours, at the peak frequency ($f = 6$), for low and high aspect ratios ($AR = 0.2$ and 0.8) and $\phi = 0.2$, $Ra = 10^6$, $A = 2$, $Ha = 100$ are depicted in Fig. 11 ($Ha = 25$) and Fig. 12 ($Ha = 100$).

Observing the streamline contours in Fig. 11, at $Ha = 25$ and for a low aspect ratio, the streamlines show a large recirculation cell formed and expanding into the upper corners and

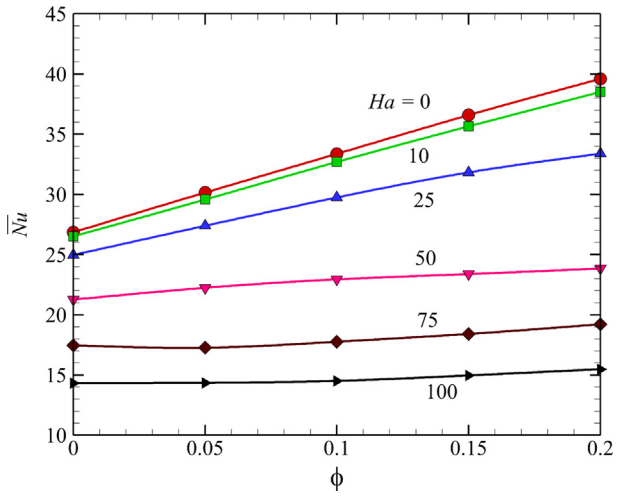

Fig. 9 $\bar{Nu}$ variation with ϕ for selected *Ha*, at $f = 6$, with $AR = 0.2$, $Ra = 10^6$ and $A = 2$. Data are fitted with cubic splines for guidance.

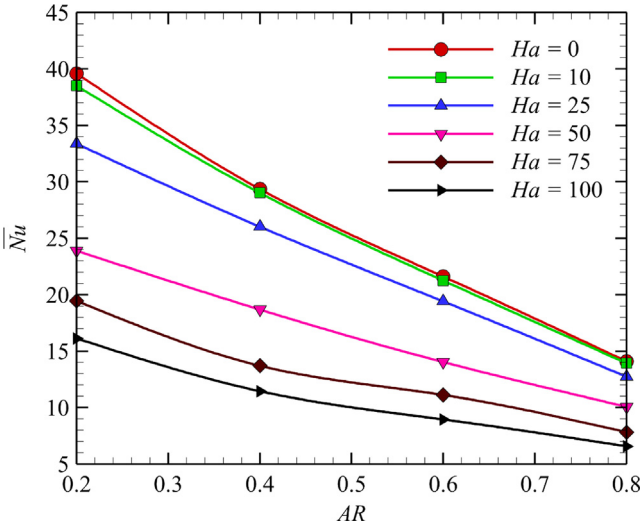

Fig. 10 $\bar{Nu}$ variation with AR for selected Ha, at $f = 6$, with $\phi = 0.2$, $Ra = 10^6$ and $A = 2$. Data are fitted with cubic splines for guidance.

the lower-left corner of the enclosure with a secondary counterrotating cell in the middle of the lower part of the enclosure. However, for a high aspect ratio, the recirculating cell expands further between the vertical walls, and the secondary counter-rotating cell in the corner becomes more active, establishing a clockwise rotating vortex. In Fig. 12, at $Ha = 100$ and $AR = 0.2$, two clockwise rotating vortices are created within the enclosure, while only one large clockwise rotating vortex is formed at $AR = 0.8$. The increase *Ha* increases Lorentz force that suppresses the formation of flow vortexes, which in turn weakens the convection heat transfer, while the conduction governs thermal energy transport, consequently, lowering $\bar{Nu}$ as was depicted in Fig. 10. It is found that the vortices in the streamlines become less dense with increasing

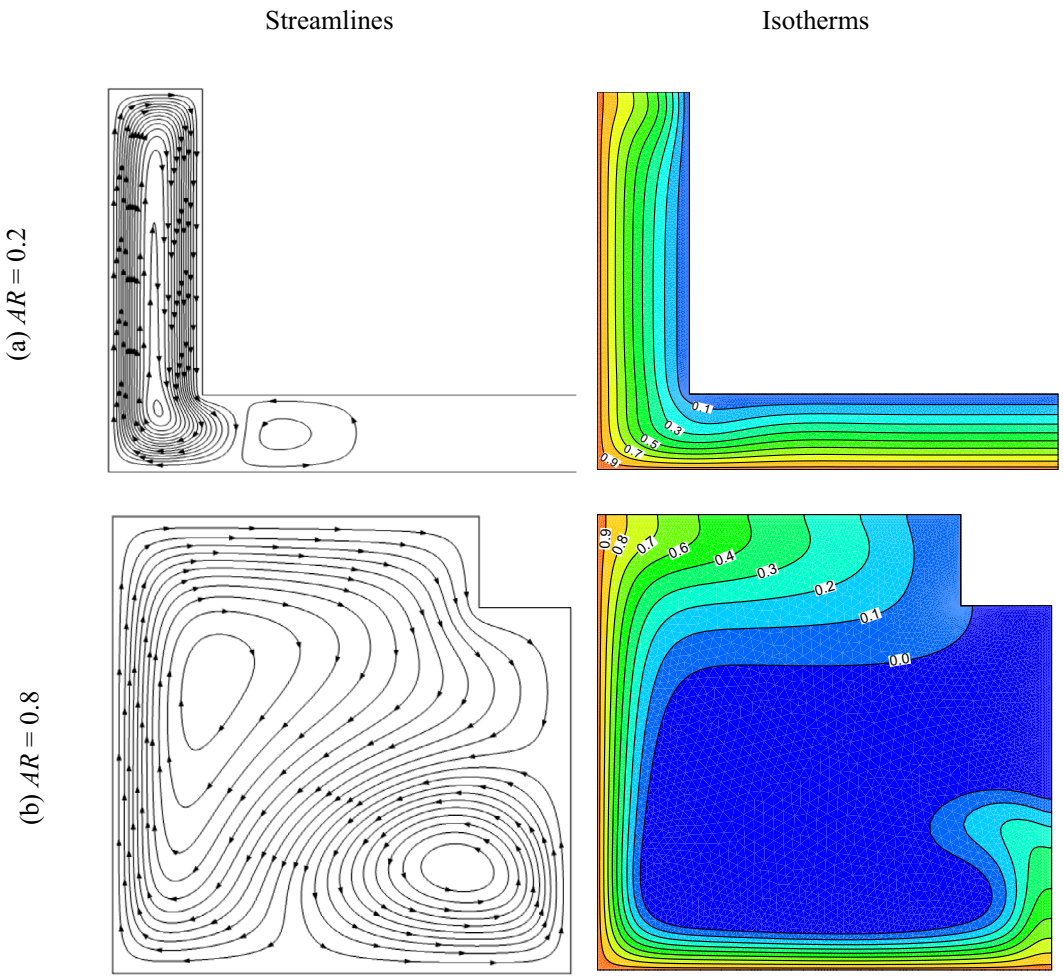

Fig. 11 Instantaneous streamlines and isotherms contours at $f = 6$ for high and low AR values after one oscillation period and $\phi = 0.2$, $Ra = 10^6$, $A = 2$, $Ha = 25$ (a) $AR = 0.2$, and (b) $AR = 0.8$.

the aspect ratio for both $Ha = 25$ and 100, resulting in a substantial variation in the transfer of heat and hence in $\bar{Nu}$.

Observing the isotherms contours presented in Figs. 11 and 12, it is clearly shown that a visible thermal boundary layer is formed near the two hot walls with nearly parallel isotherms. However, for $Ha = 25$ and $AR = 0.2$, an extreme isotherm distortion is kept in the upper corners and the lower-left corner of the enclosure, due to the formation of the recirculation cell and vortices.

5. Conclusions

In this study, free convection heat transfer of copper–water nanofluid inside an L-shaped cavity has been investigated numerically for a sinusoidal oscillating hot wall temperature in the presence of a magnetic field. The effects of enclosure aspect ratio, Rayleigh number, the volume fraction of the copper nanoparticles, the amplitudes of temperature oscillation, forcing frequencies, and Hartmann number, on the flow dynamics and transfer of heat behaviors have been investigated at a Prandtl number $Pr = 6.2$.

The natural convection was consistently enhanced by the use of nanofluid, with a 47 % increase in $\bar{Nu}$ from $\phi = 0$ to 0.2 at $Ha = 0$ and decreases to the smaller 8 % increase as Ha is ascended to $Ha = 100$.

The results showed that the higher the temperature oscillation amplitude applied to the hot walls, the higher the peak Nusselt number significantly improves heat transfer. In contrast to the square cavity case, the frequency at which the peak $\bar{Nu}$ occurs stays nearly fixed as the oscillation amplitude grows.

For $AR = 0.2$, heat transfer curried out mainly through conduction at $Ra = 10^3 - 10^5$, and $\bar{Nu}$ is unrelated to both Hartmann and Rayleigh numbers. Convection effects, on the other hand, become significant at high Rayleigh numbers, and $\bar{Nu}$ demonstrates Ha independence. The critical Rayleigh number for the transition from conduction to convection exhibits a power-law relationship. For low Hartmann number, at $Ra = 10^4$, a single clockwise rotating vortex is evolved within the vertical segment of the enclosure, whereas the fluid in the horizontal segment is approximately stagnant. For $Ra = 10^6$, Rayleigh-Bénard like cell is induced in the horizontal enclosure segment. However, for $Ra = 10^8$, the Rayleigh-

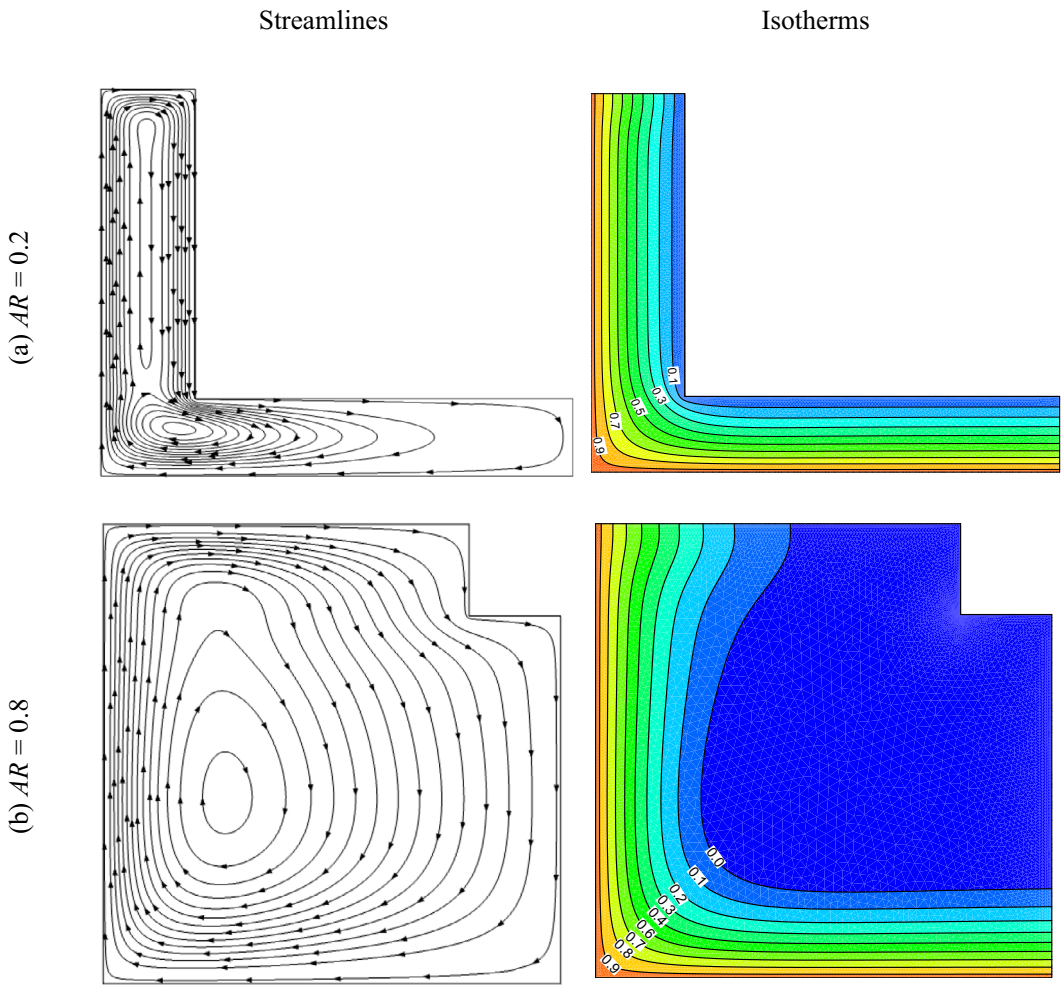

Fig. 12 Instantaneous streamlines and isotherms contours at $f = 6$ for high and low AR values after one oscillation period and $\phi = 0.2$, $Ra = 10^6$, $A = 2$, $Ha = 100$ (a) $AR = 0.2$, and (b) $AR = 0.8$.

Bénard like cells change to three. This is nearly-three orders of magnitudes more than the natural onset of the Rayleigh-Bénard instability, where $Ra_{cr} = 1708$. For $Ha = 25$, the shifting from conduction to convection happens beyond $Ra = 10^6$, while for $Ha = 100$, the flow is governed by the conduction mechanism up to $Ra = 10^6$, then by the convection mechanics beyond $Ra = 10^8$.

The streamlines are dominated by a recirculating cell, expanding further between the vertical walls. The secondary counterrotating cell in the corner becomes more active, establishing a clockwise rotating vortex for a high aspect ratio at $Ha = 25$. However, for $Ha = 100$, only one large clockwise rotating vortex is formed at $AR = 0.8$, as a consequence of increased Lorentz force that suppresses the formation of flow vortexes, enhancing the conduction over the convection heat transfer, and reducing $\bar{Nu}$. The vortices in the streamlines become denser for $Ha = 25$ and 100. The decrease in aspect ratio from 0.8 to 0.2 resulted in a significant variation in heat transfer and, thus, in $\bar{Nu}$.

The investigation showed that the solid volume fraction value effect on $\bar{Nu}$ is strongly present under low Ha values. For Hartmann number values of 0 and 50, the Nusselt number augments linearly with enlarging nanoparticles' loading, while it remained constant at $Ha = 75$ and 100.

The heat transfer increases as the aspect ratio decreases, and this increase becomes more pronounced in the range of $Ha \leq 25$, while the Nusselt number is found to be unaffected by AR for $Ha \leq 10$. Additionally, the difference in $\bar{Nu}$ between the cases of $Ha = 0$ versus $Ha = 100$ decreases with an increase in AR.

Declaration of Competing Interest

The authors declare that they have no known competing financial interests or personal relationships that could have appeared to influence the work reported in this paper.

References

[1] M. Molana, V. Zarrinderafsh, A.J. Chamkha, S. Izadi, S. Rafizadeh, Magnetohydrodynamics convection in nanofluids-filled cavities: A review, Heat Transf. - Asian Res. 49 (3) (2020) 1418–1443.
[2] A.D. Abdulsahib, K. Al-Farhany, Review of the Effects of Stationary/Rotating Cylinder in a Cavity on the Convection

Heat Transfer in Porous Media with/without Nanofluid, Math. Model. Eng. Probl. 8 (3) (2021) 356–364.
[3] M.S. Sadeghi, N. Anadalibkhah, R. Ghasemiasl, T. Armaghani, A.S. Dogonchi, A.J. Chamkha, H. Ali, A. Asadi, On the natural convection of nanofluids in diverse shapes of enclosures: an exhaustive review, J. Therm. Anal. Calorim. 147 (1) (2022) 1–22.
[4] M. Gürdal, K. Arslan, E. Gedik, A.A. Minea, Effects of using nanofluid, applying a magnetic field, and placing turbulators in channels on the convective heat transfer: A comprehensive review, Renew. Sustain. Energy Rev. 162 (2022), https://doi.org/10.1016/J.RSER.2022.112453 112453.
[5] M. Dehbani, M. Rahimi, Z. Rahimi, A review on convective heat transfer enhancement using ultrasound, Appl. Therm. Eng. 208 (2022) 118273.
[6] T. Cholewa, M. Dell'Isola, L. Canale, G. Ficco, P. Michnikowski, A. Siuta-Olcha, A. Olszewska, G. Sadowska, M.R. Dudzińska, On the influence of heat cost allocation on operation of heating system in buildings and possible, additional decrease of supply temperature, Energy Build. 254 (2022) 111599.
[7] D. Kashyap, A.K. Dass, Effect of boundary conditions on heat transfer and entropy generation during two-phase mixed convection hybrid Al2O3-Cu/water nanofluid flow in a cavity, Int. J. Mech. Sci. 157-158 (2019) 45–59.
[8] S.A. Nada, M.A. Said, Effects of fins geometries, arrangements, dimensions and numbers on natural convection heat transfer characteristics in finned-horizontal annulus, Int. J. Therm. Sci. 137 (2019) 121–137.
[9] M. Samadifar, D. Toghraie, Numerical simulation of heat transfer enhancement in a plate-fin heat exchanger using a new type of vortex generators, Appl. Therm. Eng. 133 (2018) 671–681.
[10] S.R. Bhopalam, D.A. Perumal, Numerical analysis of fluid flows in L-Shaped cavities using Lattice Boltzmann method, Appl. Eng. Sci. 3 (2020) 100016.
[11] T.S. Chang, Y.L. Tsay, Natural convection heat transfer in an enclosure with a heated backward step, Int. J. Heat Mass Transf. 44 (2001) 3963–3971, https://doi.org/10.1016/S0017-9310(01)00035-7.
[12] M. Saidi, G. Karimi, Free convection cooling in modified L-shape enclosures using copper-water nanofluid, Energy. 70 (2014) 251–271, https://doi.org/10.1016/j.energy.2014.03.121.
[13] K. Al-Farhany, K.K. Al-Chlaihawi, M.F. Al-dawody, N. Biswas, A.J. Chamkha, Effects of fins on magnetohydrodynamic conjugate natural convection in a nanofluid-saturated porous inclined enclosure, Int. Commun. Heat Mass Transf. 126 (2021) 105413.
[14] H.I. Khalaf, K.B. Saleem, K. Al-Farhany, W. Al-Kouz, Double-diffusive Air-CO2 mixture flow in a staggered cavity with numerous concave lower wall aspect ratios, Eur. Phys. J. Plus. 136 (2021), https://doi.org/10.1140/epjp/s13360-021-01486-w.
[15] W. Aich, R. Chaabane, H. Öztop, M.A. Almeshaal, C. Maatki, O. Kahouli, L. Kolsi, Numerical simulation of buoyancy-induced heat transfer and entropy generation in 3D C-shaped cavity filled with CNT–Al2O3/water hybrid nanofluid, Int. J. Nonlinear Sci. Numer. Simul. 0 (0) (2022), https://doi.org/10.1515/ijnsns-2021-0246.
[16] A.K. Hussein, H.K. Hamzah, F.H. Ali, M. Afrand, Natural convection in F-shaped cavity filled with Ag-water non-Newtonian nanofluid saturated with a porous medium and subjected to a horizontal periodic magnetic field, Korean J. Chem. Eng. 39 (4) (2022) 887–901.
[17] S. Xia, M. Mostafavi, T. Alghazali, S. sadi, J. William Grimaldo Guerrero, W. Suksatan, D. Toghraie, A. Khan, Numerical investigation of nanofluid mixed convection in a T-shaped cavity by considering a thermal barrier, Alexandria Eng. J. 61 (9) (2022) 7393–7415.
[18] T. Islam, M. Yavuz, N. Parveen, M.d. Fayz-Al-Asad, Impact of Non-Uniform Periodic Magnetic Field on Unsteady Natural Convection Flow of Nanofluids in Square Enclosure, Fractal Fract. 6 (2) (2022) 101.
[19] M. Mahmoodi, Numerical simulation of free convection of a nanofluid in L-shaped cavities, Int. J. Therm. Sci. 50 (2011) 1731–1740, https://doi.org/10.1016/J.IJTHERMALSCI.2011.04.009.
[20] E. Sourtiji, S. Hosseinizadeh, Heat transfer augmentation of magnetohydrodynamics natural convection in L-shaped cavities utilizing nanofluids, Therm. Sci. 16 (2) (2012) 489–501.
[21] M. Kalteh, H. Hasani, Lattice Boltzmann simulation of nanofluid free convection heat transfer in an L-shaped enclosure, Superlattices Microstruct. 66 (2014) 112–128.
[22] B. Mliki, M.A. Abbassi, K. Guedri, A. Omri, Lattice Boltzmann simulation of natural convection in an L-shaped enclosure in the presence of nanofluid, Eng. Sci. Technol. an Int. J. 18 (3) (2015) 503–511.
[23] B. Mliki, M. Abbassi, A. Omri, Lattice boltzmann simulation of magnethydrodynamics natural convection in an L-Shaped enclosure, Int. J. Heat Technol. 34 (4) (2016) 565–573.
[24] R. Mohebbi, M.M. Rashidi, Numerical simulation of natural convection heat transfer of a nanofluid in an L-shaped enclosure with a heating obstacle, J. Taiwan Inst. Chem. Eng. 72 (2017) 70–84.
[25] M. Sheikholeslami, A.J. Chamkha, P. Rana, R. Moradi, Combined thermophoresis and Brownian motion effects on nanofluid free convection heat transfer in an L-shaped enclosure, Chinese J. Phys. 55 (6) (2017) 2356–2370.
[26] A. Rahimi, A. Kasaeipoor, E.H. Malekshah, A. Amiri, Natural convection analysis employing entropy generation and heatline visualization in a hollow L-shaped cavity filled with nanofluid using lattice Boltzmann method- experimental thermo-physical properties, Phys. E Low-Dimensional Syst. Nanostructures. 97 (2018) 82–97.
[27] P. Zhang, M.A. Ashraf, Z. Liu, W.-X. Peng, D. Ross, The coupled lattice Boltzmann simulation of free convection in a finned L-shaped cavity filled with nanofluid, Int. J. Numer. Methods Heat Fluid Flow. 30 (3) (2020) 1478–1496.
[28] R. Mohebbi, M. Izadi, H. Sajjadi, A.A. Delouei, M.A. Sheremet, Examining of nanofluid natural convection heat transfer in a Γ-shaped enclosure including a rectangular hot obstacle using the lattice Boltzmann method, Phys. A Stat. Mech. Its Appl. 526 (2019), https://doi.org/10.1016/j.physa.2019.04.067.
[29] T. Armaghani, A.M. Rashad, O. Vahidifar, S.R. Mishra, A.J. Chamkha, Effects of discrete heat source location on heat transfer and entropy generation of nanofluid in an open inclined L-shaped cavity, Int. J. Numer. Methods Heat Fluid Flow. 29 (4) (2019) 1363–1377.
[30] M. Ghalambaz, S.A.M. Mehryan, A.I. Alsabery, A. Hajjar, M. Izadi, A. Chamkha, Controlling the natural convection flow through a flexible baffle in an L-shaped enclosure, Meccanica. 55 (8) (2020) 1561–1584.
[31] R. Zhang, S. Aghakhani, A. Hajatzadeh Pordanjani, S.M. Vahedi, A. Shahsavar, M. Afrand, Investigation of the entropy generation during natural convection of Newtonian and non-Newtonian fluids inside the L-shaped cavity subjected to magnetic field: application of lattice Boltzmann method, Eur. Phys. J. Plus. 135 (2020), https://doi.org/10.1140/epjp/s13360-020-00169-2.
[32] S.E. Ahmed, M.A. Mansour, A.M. Alwatban, A.M. Aly, Finite element simulation for MHD ferro-convective flow in an

inclined double-lid driven L-shaped enclosure with heated corners, Alexandria Eng. J. 59 (1) (2020) 217–226.
[33] S.M. Seyyedi, A.S. Dogonchi, M. Hashemi-Tilehnoee, M. Waqas, D.D. Ganji, Entropy generation and economic analyses in a nanofluid filled L-shaped enclosure subjected to an oriented magnetic field, Appl. Therm. Eng. 168 (2020) 114789.
[34] S. Naseri Nia, F. Rabiei, M.M. Rashidi, T.M. Kwang, Lattice Boltzmann simulation of natural convection heat transfer of a nanofluid in a L-shape enclosure with a baffle, Results Phys. 19 (2020) 103413.
[35] S. Mojumder, S. Saha, M. Rizwanur Rahman, M.M. Rahman, K.M. Rabbi, T.A. Ibrahim, Numerical study on mixed convection heat transfer in a porous L-shaped cavity, Eng. Sci. Technol. an Int. J. 20 (1) (2017) 272–282.
[36] A.J. Chamkha, G. Jomardiani, M.A. Ismael, R. Ghasemiasl, T. Armaghani, Thermal and entropy analysis in L-shaped non-Darcian porous cavity saturated with nanofluids using Buongiorno model: Comparative study, Math. Methods Appl. Sci. (2020), https://doi.org/10.1002/mma.6797.
[37] H. Moria, Natural convection in an L-shape cavity equipped with heating blocks and porous layers, Int. Commun. Heat Mass Transf. 126 (2021) 105375.
[38] M.A. Almeshaal, C. Maatki, L. Kolsi, K. Ghachem, A. Chamkha, 3D Rayleigh-Bénard-type natural convection in MWCNT-nanofluid-filled L-shaped enclosures with consideration of aggregation effect, Math. Methods Appl. Sci. (2020), https://doi.org/10.1002/mma.6409.
[39] H. Mohammadifar, H. Sajjadi, M. Rahnama, S. Jafari, Y. Wang, Investigation of Nanofluid Natural Convection Heat Transfer in Open Ended L-shaped Cavities utilizing LBM, J. Appl. Comput. Mech. 7 (2021), https://doi.org/10.22055/JACM.2020.33495.2235.
[40] X.H. Zhang, T. Saeed, E.A. Algehyne, M.A. El-Shorbagy, A.M. El-Refaey, M. Ibrahim, Effect of L-shaped heat source and magnetic field on heat transfer and irreversibilities in nanofluid-filled oblique complex enclosure, Sci. Rep. 11 (2021), https://doi.org/10.1038/s41598-021-95803-z.
[41] T. Armaghani, M.S. Sadeghi, A.M. Rashad, M.A. Mansour, A. J. Chamkha, A.S. Dogonchi, H.A. Nabwey, MHD mixed convection of localized heat source/sink in an Al2O3-Cu/water hybrid nanofluid in L-shaped cavity, Alexandria Eng. J. 60 (3) (2021) 2947–2962.
[42] S.A. Kumar, K.S. Meenakshi, B.R.V. Narashimhan, S. Srikanth, G. Arthanareeswaran, Synthesis and characterization of copper nanofluid by a novel one-step method, Mater. Chem. Phys. 113 (1) (2009) 57–62.
[43] G. Wang, X. Meng, M. Zeng, H. Ozoe, Q.W. Wang, Natural convection heat transfer of copper-water nanofluid in a square cavity with time-periodic boundary temperature, Heat Transf. Eng. 35 (6-8) (2014) 630–640.
[44] P.A. Davidson (Ed.), An Introduction to Magnetohydrodynamics, Cambridge University Press, 2001.
[45] M. Pirmohammadi, M. Ghassemi, G.A. Sheikhzadeh, Effect of a magnetic field on buoyancy-driven convection in differentially heated square cavity, IEEE Trans. Magn. (2009), https://doi.org/10.1109/TMAG.2008.2008685.
[46] K. Khanafer, K. Vafai, M. Lightstone, Buoyancy-driven heat transfer enhancement in a two-dimensional enclosure utilizing nanofluids, Int. J. Heat Mass Transf. 46 (2003) 3639–3653, https://doi.org/10.1016/S0017-9310(03)00156-X.
[47] K. Khanafer, K. Vafai, A critical synthesis of thermophysical characteristics of nanofluids, Int. J. Heat Mass Transf. 54 (2011) 4410–4428, https://doi.org/10.1016/J.IJHEATMASSTRANSFER.2011.04.048.
[48] Y. Xuan, W. Roetzel, Conceptions for heat transfer correlation of nanofluids, Int. J. Heat Mass Transf. 43 (2000) 3701–3707, https://doi.org/10.1016/S0017-9310(99)00369-5.
[49] H.C. Brinkman, The viscosity of concentrated suspensions and solutions, J. Chem. Phys. 20 (4) (1952) 571.
[50] W. Yu, S.U.S. Choi, The role of interfacial layers in the enhanced thermal conductivity of nanofluids: A renovated Hamilton-Crosser model, J. Nanoparticle Res. 6 (4) (2004) 355–361.
[51] W.K. Hussam, K. Khanafer, H.J. Salem, G.J. Sheard, Natural convection heat transfer utilizing nanofluid in a cavity with a periodic side-wall temperature in the presence of a magnetic field, Int. Commun. Heat Mass Transf. 104 (2019) 127–135.